Title
Effect of Pathogenic Mutations on the Formation of High-Order Dynamin 2 Assemblies in Living Cells

Journal
Biochemistry, 63(21)

ISSN
0006-2960

Authors
Hedde, Per Niklas
Zhu, Songning
Barylko, Barbara
et al.

Publication Date
2024-11-05

DOI
10.1021/acs.biochem.4c00262

Biochemistry

pubs.acs.org/biochemistry Article

Effect of Pathogenic Mutations on the Formation of High-Order Dynamin 2 Assemblies in Living Cells

Per Niklas Hedde, Songning Zhu, Barbara Barylko, Chi-Li Chiu, Luke T. Nelson, Michelle A. Digman, Joseph P. Albanesi, Nicholas G. James,* and David M. Jameson*

Cite This: *Biochemistry* 2024, 63, 2750−2758 Read Online

ACCESS | Metrics & More | Article Recommendations | Supporting Information

ABSTRACT: Mutations in dynamin 2 (DNM2) have been associated with two distinct movement disorders: Charcot-Marie-Tooth neuropathies (CMT) and centronuclear myopathy (CNM). Most of these mutations are clustered in the pleckstrin homology domain (PHD), which engages in intramolecular interactions that limit dynamin self-assembly and GTPase activation. CNM mutations interfere with these intramolecular interactions and suppress the formation of the autoinhibited state. CMT mutations are located primarily on the opposite surface of the PHD, which is specialized for phosphoinositide binding. It has been speculated that the distinct locations and interactions of residues mutated in CMT and CNM explain why each set of mutations causes either one disease or the other, despite their close proximity within the PHD sequence. We previously reported that at least one CMT-causing mutant, lacking residues $_{555}$DEE$_{557}$ (ΔDEE), displays the same inability to undergo autoinhibition as observed in CNM-linked mutants. Here, we show that both the DNM2$^{\Delta DEE}$ and CNM-linked DNM2^{A618T} mutants form larger and more stable structures on the plasma membrane than that of wild-type DNM2 (DNM2^{WT}). However, DNM2^{A618T} forms cytoplasmic inclusions at concentrations lower than those of either DNM2^{WT} or DNM2$^{\Delta DEE}$, suggesting that CNM-linked mutations confer more severe gain-of-function properties than the ΔDEE mutation.

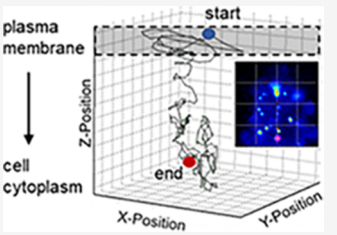

INTRODUCTION

Dynamins are ∼100 kDa GTPases that catalyze membrane scission[1,2] and regulate actin polymerization.[3,4] Mammalian cells express three dynamin isoforms: dynamin 1 (DNM1), which is enriched in presynaptic nerve terminals and promotes synaptic vesicle recycling; dynamin 2 (DNM2), which is ubiquitously expressed and accounts for most examples of receptor-mediated endocytosis, and dynamin 3 (DNM3), which is enriched in postsynaptic nerve terminals and may participate in the organization of dendritic spines.[5,6] The three isoforms have a similar domain organization, including an N-terminal GTPase "head" domain, a "middle" domain consisting of an antiparallel three-helix bundle, a phosphoinositide-binding pleckstrin homology domain (PHD), an α-helical GTPase effector domain (GED) that folds back onto the middle domain to form the "stalk", and a C-terminal proline/arginine-rich domain that interacts with SH3-domain-containing proteins. Dynamin self-assembly, which involves stalk−stalk and head−head interactions, stimulates GTPase activity from basal levels of ∼1−10 min^{-1} to over 200 min^{-1}. Structural studies have revealed that dynamins can adopt two conformations: an assembly competent extended ("open") conformation, in which the PHD can bind to membranes, and an autoinhibited ("closed") conformation, in which the PHD folds back onto the stalk and sterically blocks self-assembly.[7−9]

Mutations in DNM2 have been identified in patients with two neuromuscular disorders, Charcot-Marie-Tooth disease (CMT)[10,11] and centronuclear myopathy (CNM),[12,13] which affect nerves and muscles, respectively. There is almost no overlap between the sets of mutations that cause these two disorders, suggesting that they have distinct effects on the activity or regulation of DNM2. We previously reported that several CNM-linked DNM2 mutations, including R369W in the middle domain and A618T in the PHD, induce the formation of stable DNM2 polymers that are abnormally resistant to disassembly by salt and GTP.[14] Kenniston and Lemmon reported similar findings and proposed that CNM mutations disrupt allosteric regulation of DNM2 GTPase activity by the PHD.[15] They further demonstrated that the most prevalent CMT-causing mutation, K562E, did not enhance dynamin polymerization or GTPase activation but instead suppressed phosphatidylinositol (4,5)-bisphosphate (PIP_2) binding and PIP_2-stimulated GTPase activity. Subsequent structural analysis of the closed DNM1 conformation provided an explanation for these observations, as residues mutated in CNM were found to be clustered at the PHD-stalk interface, whereas residues mutated in CMT were clustered on the opposite surface of the PHD, which drives PIP_2 binding.[7,8] Thus, CNM mutations are apparently hypermorphic due to

Received: May 15, 2024
Revised: October 4, 2024
Accepted: October 4, 2024
Published: October 11, 2024

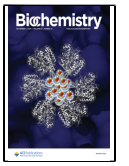

https://doi.org/10.1021/acs.biochem.4c00262
Biochemistry 2024, 63, 2750−2758

their disruption of autoinhibitory PHD-stalk interactions, whereas CMT mutations are apparently hypomorphic due to their disruption of activating PHD−PIP_2 interactions. Consistent with these molecular properties, DNM2-dependent CNM and CMT are currently viewed as gain-of-function and loss-of function disorders, respectively.[16−20]

We recently reported that at least one CMT mutant ($DNM2^{\Delta DEE}$), which lacks residues $_{555}DEE_{557}$ in the PIP_2-binding surface of the PHD, shares several *in vitro* properties with CNM-linked mutants.[21] Like the CNM mutants, $DNM2^{\Delta DEE}$ forms stable polymers that express high PIP_2-independent GTPase activity *in vitro*, and its PHD binds to PIP_2 as strongly as the PHD of wild type DNM2 ($DNM2^{WT}$). However, we also observed that in contrast to the CNM mutants, which form oligomers containing up to 20−25 DNM2 monomers in the cytoplasm of living cells, $DNM2^{\Delta DEE}$ does not self-assemble beyond the predominant dimer-tetramer equilibrium characteristic of $DNM2^{WT}$. Although $DNM2^{\Delta DEE}$ shares some hypermorphic characteristics with the CNM-linked DNM2 mutants, it should be noted that the mutation itself originates from a deletion at the 3′ end of DNM2 that generates both a frameshift and the in-frame deletion that leads to $DNM2^{\Delta DEE}$ production.[10] As a result, the mutation results in a profound decrease in DNM2 expression,[10] which would be consistent with the loss-of-function nature of DNM2-related CMT.[20] In the present study, we extended our analysis of the behavior of $DNM2^{\Delta DEE}$ in live cells, focusing on its behavior at the cell periphery and on its propensity to incorporate into large cytoplasmic inclusions. Our data suggest that in cells $DNM2^{\Delta DEE}$ displays properties intermediate between those of $DNM2^{WT}$ and CNM-linked DNM2 mutants.

MATERIALS AND METHODS

Cell Culture. HEK293 and NIH-3T3 cells were cultured in DMEM (supplemented with 10% FBS and 1% Pen-Strep), plated on fibronectin-coated glass-bottom dishes (No. 1.5), and transfected with Lipofectamine 2000 or 3000 (ThermoFisher, Waltham, MA). Cells were imaged at 18−28 h after transfection.

Constructs. Each fluorescent DNM2 construct utilized was cloned into the pEGFP-N1 vector (Clontech) as described elsewhere[21] to generate C-terminal EGFP fusion constructs.

Confocal Imaging. NIH-3T3 cells were transfected with plasmids encoding either $DNM2^{WT}$, $DNM2^{\Delta DEE}$, or $DNM2^{A618T}$ and imaged at 37 °C and 5% CO_2 with an LSM880 laser scanning microscope (Zeiss, Jena, Germany). EGFP fluorescence was excited at 488 nm and collected in a band of 510−560 nm with a 40×, NA 1.2 water immersion lens and focused on a pinhole set to one Airy unit before detection with a photomultiplier detector. Images of 1,024 × 1,024 pixels were acquired with a pixel size of 83 nm. All imaging parameters were kept constant during the experiment such that photon counts in each pixel were proportional to the fluorescent protein levels.

Fluorescence Recovery after Photobleaching (FRAP). HEK293T cells were transfected with plasmids encoding $DNM2^{WT}$ and $DNM2^{\Delta DEE}$ and imaged at 37 °C and 5% CO_2 with a LSM880 laser scanning microscope (Zeiss) set up for FRAP. EGFP fluorescence was excited at 488 nm and detected in a band of 510−560 nm with a 40×, NA 1.2 water immersion lens. In each data set, one prebleaching and 34 postbleaching frames of 256 × 256 pixels were acquired at 1.25 s intervals with a pixel size of 138 nm. EGFP was bleached in 1−3 circular regions per cell of 1−2 μm diameter for 0.3−1 s each by using 100% laser power. Data were analyzed in Origin (OriginLab, MA). A single exponential association model was used to calculate the recovery times for each experiment.

Total Internal Reflection Microscopy (TIRFM). HEK293T cells were transfected with plasmids encoding either $DNM2^{WT}$-EGFP, $DNM2^{\Delta DEE}$-EGFP, $DNM2^{R369W}$-EGFP, or $DNM2^{A618T}$-EGFP and imaged at room temperature with an Olympus IX81 instrument (Olympus) equipped with a TIRF illumination module. EGFP fluorescence was excited with 488 nm light at the critical angle, collected in a band of 510−540 nm with a 60×, NA 1.45 oil immersion lens and, after an additional 2× magnification (total magnification 120×), imaged with a Prime95B (Photometrics) sCMOS camera. Per image, 10 frames were acquired with 100 ms exposure time and averaged before analysis.

3D Orbital Tracking. The hardware and software for the three-dimensional single particle tracking (3D-SPT) routine were implemented on a FV1000 (Olympus, Center Valley, PA) confocal microscope as previously described.[22,23] The galvano scanner and z-nanodrive of the microscope were driven by an IOtech DAC card (MCC, Norton, MA) to control the laser beam position. HEK293 cells, which were plated onto fibronectin-coated No 1.5 cover-glass imaging dishes, were transfected with DNM2 constructs using Lipofectamine 2000. Cells were imaged with a 40× 0.8 NA water immersion objective with a working distance of 3 mm. The argon-ion laser of the Olympus FV1000 was set to an excitation wavelength of 488 nm (0.1% power) to excite EGFP and the emission was collected in a band between 505 and 605 nm. The fluorescence intensity at 128 points along a circular orbit was collected with a pixel dwell time of 128 μs (16.4 ms/orbit). All tracking data were analyzed using SimFCS software (available at: https://www.lfd.uci.edu/globals/).

Spot Quantification. The size and the intensity were quantified using the Python script. Image was median-filtered in windows of 3 pixels to create a denoised image (MED) and 15 pixels to create a low-pass filtered image (MED25). A background value (BKG) is determined where there is no fluorescent. A binary mask is created using THRESH = MED − 1.5 × MED25-BKG, following by a nonzero threshold. Each punctum is then identified as having more than 8 nonzero neighbor elements. Within each puncta, its area and intensity are measured.

RESULTS

The CMT-Associated $DNM2^{\Delta DEE}$ Mutant Forms Large, Stable Structures on the Plasma Membrane. In a prior investigation, we used fluorescence fluctuation spectroscopy in the total internal reflection fluorescence mode (TIRF-FFS) to determine how the CNM-associated mutation R369W affects the size and dynamics of DNM2 on the plasma membrane (PM).[24] TIRF microscopy (TIRFM) utilizes the evanescent field generated from a beam, which has undergone total internal reflection at the sample/glass interface to generate fluorescence from a very thin (<100 nm) layer and, hence, is ideally suited for investigation of dynamic processes occurring within or near the PM. We reported that PM puncta containing $DNM2^{R369W}$-EGFP were, on average, larger than those containing $DNM2^{WT}$-EGFP. To determine if $DNM2^{\Delta DEE}$ also incorporates into large peripheral puncta, we examined HEK293 cells expressing $DNM2^{WT}$-EGFP,

https://doi.org/10.1021/acs.biochem.4c00262
Biochemistry 2024, 63, 2750−2758

DNM2$^{\Delta DEE}$-EGFP, and DNM2^{R369W} using TIRFM. Visual inspection of the images (Figure 1) suggests that both

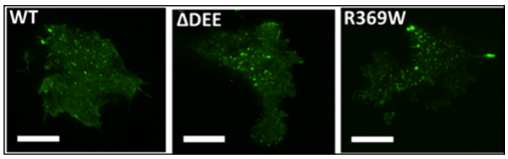

Figure 1. Analysis of peripheral DNM2-EGFP-containing puncta in HEK293 cells using TIRF microscopy. Cells were transfected with DNM2^{WT}-EGFP, DNM2$^{\Delta DEE}$-EGF, or DNM2^{R369W}-EGFP. Scale bar, 20 μm.

DNM2$^{\Delta DEE}$ and DNM2^{R369W} incorporate into slightly larger peripheral puncta than does DNM2^{WT}. We next sought to quantify the differences in size of peripheral puncta containing EGFP-tagged DNM2^{WT}, DNM2$^{\Delta DEE}$, and CNM mutant DNM2^{A618T}. We chose to examine the A618T mutant in more detail both to extend our investigation beyond DNM2^{R369W} and because the A618T mutation causes a particularly severe form of CNM.[25] In Figure 2, the areas of

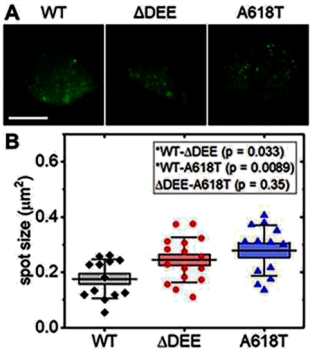

Figure 2. TIRFM analysis of DNM2-containing peripheral puncta in HEK293T cells expressing EGFP-tagged DNM2 constructs. (A) Representative TIRF images of cells transfected with DNM2^{WT}-EGFP (left), DNM2$^{\Delta DEE}$-EGFP (middle), and DNM2^{A618T}-EGFP (right). Scale bar: 20 μm. (B) Average area occupied by the inclusions. Black squares: DNM2^{WT}; red circles: DNM2$^{\Delta DEE}$; blue triangles: DNM2^{A618T}. Statistical analysis confirms that peripheral inclusion sizes for DNM2$^{\Delta DEE}$ and DNM2^{A618T} are significantly larger than those for DNM2^{WT}. *P* values (insets) were calculated with the Mann–Whitney nonparametric test; box: standard error; whiskers: standard deviation; center line: mean.

peripheral puncta containing EGFP-tagged DNM2^{WT}, DNM2$^{\Delta DEE}$, and CNM mutant DNM2^{A618T} are quantified. Both DNM2$^{\Delta DEE}$ and DNM2^{A618T} form larger PM puncta than DNM2^{WT}. Puncta formed by DNM2^{A618T} are slightly larger, on average, than those formed by DNM2$^{\Delta DEE}$.

We next used three-dimensional single-particle tracking (3D-SPT)[22,23] to determine how the ΔDEE mutation affects the dynamics of DNM2-containing PM puncta. Figure 3A shows a representative 3D-SPT time trace for DNM2^{WT}-EGFP, wherein the tracked membrane punctum (t = 0 s, highlighted in blue) was internalized in the axial direction shortly after tracking was initiated. Fluorescence was no longer detectable once the punctum had traveled ∼60 nm deep into the cytoplasm (highlighted in red). Loss of fluorescence is likely due to the disassembly of DNM2^{WT}-EGFP polymers following internalization as low-order DNM2 oligomers would not be detectable in our tracking setup. All of the DNM2^{WT}-EGFP-containing puncta reported in this work were found to track several nanometers in the axial direction (61 ± 31 nm), and their signals could no longer be tracked after about one min (80 ± 50 s). We note that the large variance in both distance and acquisition time likely results from initiating data collection at arbitrary time points within the life cycle of the membrane puncta. In Figure 3B, we show the behavior of one DNM2^{WT}-EGFP-containing punctum and one DNM2$^{\Delta DEE}$-EGFP-containing punctum, which are typical of all puncta examined. In contrast to the DNM2^{WT}-EGFP punctum, the punctum containing DNM2$^{\Delta DEE}$-EGFP hovered within about 10 nm of the PM, showing no sign of internalization. Tracking was eventually stopped after 15 min. Figure 3C relates the distance traveled by each punctum as a function of the time at which fluorescence became undetectable (for DNM2^{WT}-EGFP) or at which tracking was terminated (for DNM2$^{\Delta DEE}$-EGFP and DNM2^{R369W}-EGFP). Puncta containing DNM2$^{\Delta DEE}$-EGFP or DNM2^{R369W}-EGFP showed minimal changes within the axial direction (15 ± 10 nm), even with observation times extending to almost 20 min. Taken together, the results shown in Figures 1 and 2 demonstrate that DNM2$^{\Delta DEE}$ forms large, stable structures on the periphery of live cells, thus revealing another similarity with the CNM-linked DNM2 mutants.

Effect of Pathogenic Mutations on the Formation of Cytoplasmic DNM2-Containing Puncta. We previously reported that the CNM-associated R369W mutation increases the propensity of DNM2 to incorporate into large puncta in

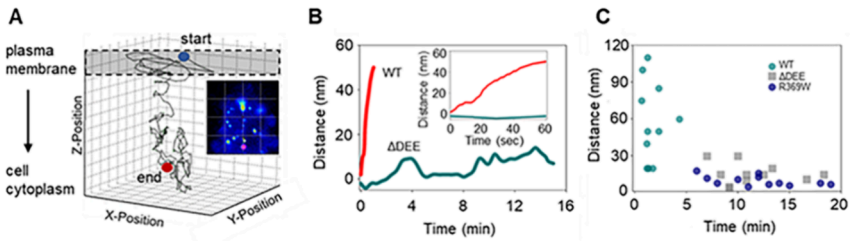

Figure 3. 3D-SPT of DNM2 membrane puncta in HEK293T cells. (A) Representative 3D-SPT time trace for DNM2^{WT} with the start and end points of the time trace marked in blue and red, respectively. The shaded area represents the membrane region. The tracked DNM2^{WT} membrane punctum was internalized shortly after tracking was initiated and no longer detectable once it had traveled ∼60 nm deep into the cytoplasm. (B) Representative time traces of one DNM2^{WT}-containing (red track) and one DNM2$^{\Delta DEE}$-containing punctum (cyan track). For the punctum containing DNM2$^{\Delta DEE}$, which hovered within ∼10 nm of the plasma membrane showing no sign of internalization, tracking was stopped after 15 min. (C) Distances traveled by 11 (DNM2^{WT}) 10 (DNM2$^{\Delta DEE}$), and 12 (DNM2^{R369W}) tracked puncta as a function of time. Tracking was stopped if fluorescence became undetectable (for DNM2^{WT}) or after 5–20 min (for DNM2$^{\Delta DEE}$ and DNM2^{R369W}). Puncta containing DNM2$^{\Delta DEE}$ or DNM2^{R369W} showed minimal changes in the axial direction (15 ± 10 nm), even for observation times over 10 min.

https://doi.org/10.1021/acs.biochem.4c00262
Biochemistry 2024, 63, 2750−2758

the cytoplasm of CV1 cells.[24] Similar observations were reported for four CNM-associated mutants (R465W, R522H, S619L, P627H) expressed in COS1 cells,[26] for the CNM-associated S619L mutant expressed in H1299 cells,[9] and for the Hereditary Spastic Paraplegia-associated R719W mutant expressed in HeLa cells.[27] In contrast, the CMT-associated G358R and K562E mutations did not enhance the incorporation of DNM2 into large puncta.[26] Although the clinical significance of these puncta remains to be defined, similar structures have been identified in biopsies from CNM patients and in animal models of CNM (see Discussion).

Considering our findings that the ΔDEE mutation confers gain-of-function properties to DNM2, we tested whether $DNM2^{\Delta DEE}$ has a greater tendency than $DNM2^{WT}$ to localize to large cytoplasmic puncta. Figure 4 qualitatively shows that

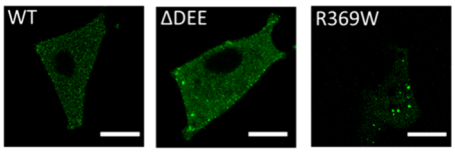

Figure 4. Formation of cytoplasmic puncta containing wild-type and mutant forms of DNM2-EGFP. HEK293 cells were transfected with constructs encoding $DNM2^{WT}$-EGFP (~440 nM), $DNM2^{\Delta DEE}$-EGFP (~400 nM), or $DNM2^{R369W}$-EGFP (~382 nM). Concentrations of expressed proteins were estimated using autocorrelation analysis of the fluorescence correlation spectroscopy data. Scale bar: 20 μm.

HEK293 cells expressing DNM^{R369W}-EGFP and $DNM^{\Delta DEE}$-EGFP contain larger fluorescent puncta than do cells expressing $DNM2^{WT}$-EGFP. Using fluorescence correlation spectroscopy, we determined that the concentrations of EGFP-tagged DNM2 (WT and mutants) in these cells were ~400 nM. To estimate the concentration of endogenous DNM2 in HEK293 cells, we immunoblotted cell extracts with anti-DNM2 antibodies (Supplementary Figure S1). Using purified DNM2-His_6 as a calibration standard, we found that HEK293 cells contain ~330 nM DNM2/cell, which is similar to the 385 nM level previously determined for HeLa cells.[28] Thus, the micrographs in Figure 4 suggest that, at total cellular DNM2 concentrations of ~700−800 nM, $DNM2^{\Delta DEE}$ and $DNM2^{R369W}$ have a higher propensity to form larger cytoplasmic inclusions than does $DNM2^{WT}$.

We carried out a quantitative comparison of cytoplasmic puncta formed in HEK293 cells by $DNM2^{WT}$, $DNM2^{\Delta DEE}$, and $DNM2^{A618T}$. In cells expressing low levels of tagged proteins, the intensity is defined as having an average of less than 500 counts/s/pixel over the whole cell (Supplementary Figure S2, top panel), $DNM2^{A618T}$ puncta are clearly more evident by confocal imaging than those formed by $DNM2^{WT}$ or $DNM2^{\Delta DEE}$ (Figure 5, left column). However, several large puncta containing $DNM2^{\Delta DEE}$ clearly appeared at high expression levels (cells with an average intensity greater than 500 counts/s/pixel; Supplementary Figure S2, bottom panel) (Figure 5, right column). Quantification of the number and area of puncta is presented in Figures 5 and 6, respectively. At both low and high expression levels, $DNM2^{A618T}$ forms more cytoplasmic puncta per cell than either $DNM2^{WT}$ or $DNM2^{\Delta DEE}$ (Figure 6A,B). At high expression levels, $DNM2^{\Delta DEE}$ forms approximately double the number of puncta as $DNM2^{WT}$ (Figure 6B). Although confocal imaging indicates that the mutant dynamins form several puncta that are much

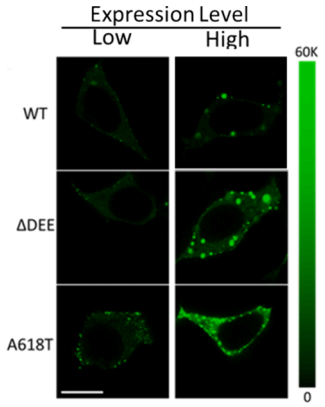

Figure 5. Representative confocal image of HEK293 cells expressing low (left column) or high (right column) levels of DNM2-EGFP constructs. Cells were transfected with $DNM2^{WT}$-EGFP (top row), $DNM2^{\Delta DEE}$-EGFP (middle row), or $DNM2^{A618T}$-EGFP (bottom row). Scale bar: 10 μm.

larger than those observed in cells expressing $DNM2^{WT}$ (Figure 5), the overall average size of puncta formed by mutant and WT dynamins is reasonably similar (Figure 7). However, $DNM2^{\Delta DEE}$ has a tendency to form larger puncta than $DNM2^{WT}$ or $DNM2^{A618T}$ at high expression levels.

We next characterized the dynamics of $DNM2^{WT}$ and $DNM2^{DEE}$ in cytoplasmic inclusions by using fluorescence recovery after photobleaching (FRAP). FRAP allowed us to investigate the exchange rate of proteins within those cytoplasmic inclusions with the surrounding environment. Figure 8 shows prebleaching (panels A and B) and postbleaching (panels C and D) fluorescence images of DNM^{WT} (panels A and C) and $DNM2^{\Delta DEE}$ (panels B and D). The photobleached puncta are marked by red circles. The average normalized fluorescence recovery data of $DNM2^{WT}$ and $DNM2^{\Delta DEE}$ (10 cells each) are displayed in Figure 6E. Statistical analysis of the recovery times obtained by fitting a single exponential association model did not reveal any significant difference between $DNM2^{WT}$ and $DNM2^{\Delta DEE}$, despite the difference in the average sizes of the inclusions formed by these proteins (Figure 5). These results demonstrate that DNM2 molecules within the puncta exchange rapidly with their counterparts in the surrounding environment.

DISCUSSION

Compelling *in vitro* data suggest that most CMT- and CNM-associated mutations confer loss-of-function and gain-of-function properties, respectively, on DNM2.[20] For example, the CMT-linked $DNM2^{G537C}$ and $DNM2^{K562E}$ mutants display reduced GTPase activation[15,16] and reduced ability to promote membrane fission.[16] In contrast, all CNM-associated DNM2 mutations characterized to date, including R369W,[14] R465W,[16] A618T,[15,16] S619L,[15,16] and S619W[15] have been found to express inordinately high levels of basal and stimulated GTPase activity. Likewise, mutations E368 K, R465W, E560 K, A618T, and S619L increase the membrane fission activity of DNM2.[16] These hypermorphic properties are likely caused by the disruption of inhibitory intramolecular stalk-PHD interactions resulting from the CNM-causing mutations.[9] Thus, as we previously showed using FFS, cytosolic $DNM2^{WT}$ is predominantly tetrameric, whereas the CNM-associated $DNM2^{R269W}$ mutant exists largely as higher-

https://doi.org/10.1021/acs.biochem.4c00262
Biochemistry 2024, 63, 2750−2758

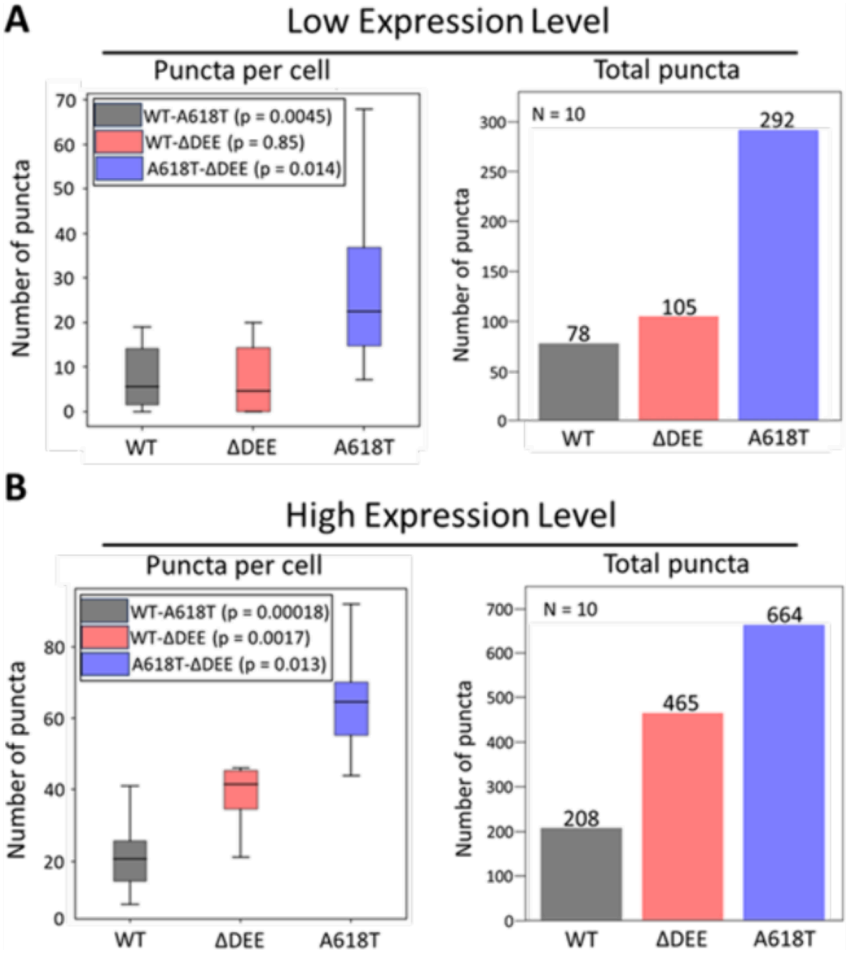

Figure 6. Comparison of the number of DNM2-containing cytoplasmic inclusions in HEK293 cells. (A) Quantification of puncta in cells expressing low levels (<500 cts/px) of DNM2-EGFP^{WT} (gray bars), DNM2-EGFP$^{\Delta DEE}$ (red bars), and DNM2-EGFP^{A618T} (blue bars). (B) Similar quantification for cells expressing high levels of EGFP-tagged dynamins (>500 cts/px). *P* values (insets) were calculated with Mann−Whitney nonparametric test; box: interquartile, lower whisker: minimum value excluding outliers, upper whisker: maximum value excluding outliers, centerline: median value.

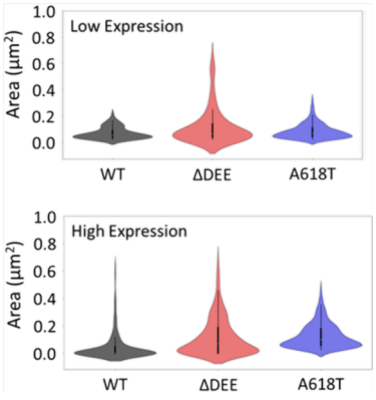

Figure 7. Size distributions of DNM2-containing cytoplasmic inclusions in HEK293 cells. At both high and low expression levels, there are multiple populations of puncta size. Small puncta are evident for all three DNM2 forms regardless of the expression level. However, more of the larger puncta form with DNM2$^{\Delta DEE}$ at low expression levels.

order oligomers in cells.[24,29] The positioning of CMT-linked mutations suggests that they should not interfere with autoinhibitory stalk-PHD interactions but instead should weaken PIP_2−PHD interactions, thereby inhibiting rather than promoting DNM2 self-assembly. Therefore, we were surprised to find that the CMT-associated ΔDEE mutation did not interfere with PIP_2 binding and that DNM2$^{\Delta DEE}$ showed enhanced PIP_2-activated GTPase activity and formed polymers that were more resistant than wild-type to disassembly by GTP and high ionic strength.[21] The distinct *in vitro* properties of DNM2$^{\Delta DEE}$ may partially explain the different phenotypes observed upon its expression vs expression of other CMT-linked DNM2 mutants in cells. For example, DNM2 constructs containing CMT-associated mutations G358R, G537C, K562E, or L570H disrupt clathrin-mediated endocytosis (CME),[30] whereas expression of DNM2$^{\Delta DEE}$ has no effect on CME.[31−33] Instead, DNM2$^{\Delta DEE}$ (but not DNM2^{K558E}, the equivalent of DNM2^{K562E} in the DNM2 isoform used in that study) has been reported to increase tubulin acetylation and to impair dynamic instability of microtubules (MTs).[31] In contrast, expression of DNM2^{K562E}, but not DNM2$^{\Delta DEE}$, results in aberrant organization of the actin cytoskeleton.[34,35]

The gain-of-function *in vitro* properties of CNM-associated DNM2 mutants are consistent with the effects of their expression in cells, animal models, and patient samples. Expression of DNM2^{R465W}, DNM2^{A618T}, and DNM2^{S619L} (but not of the CMT-linked DNM2^{G537K} mutant) induces

https://doi.org/10.1021/acs.biochem.4c00262
Biochemistry 2024, 63, 2750−2758

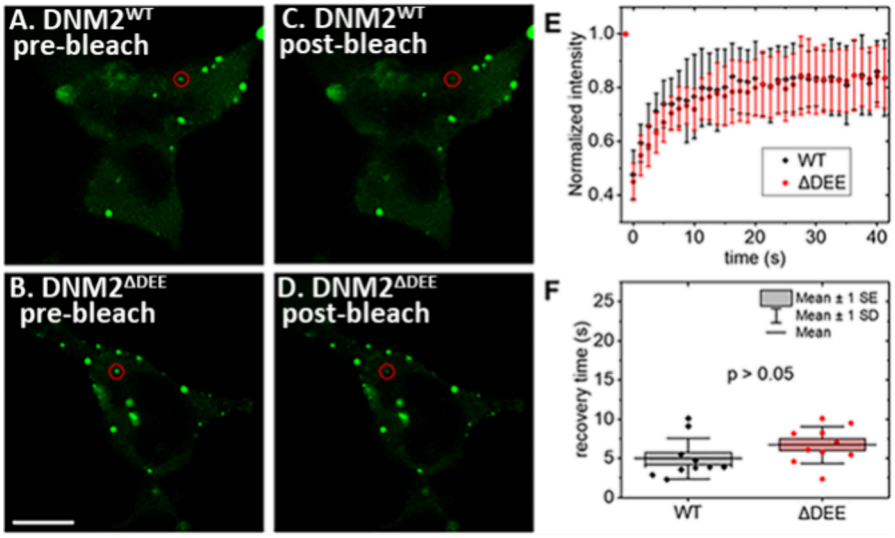

Figure 8. FRAP of cytoplasmic DNM2 inclusions in HEK293T cells. (A,B) Prebleaching and (C,D) postbleaching fluorescence images of $DNM2^{WT}$-EGFP (A,C) and $DNM2^{\Delta DEE}$-EGFP (B,D). Bleached inclusions are marked by red circles. (E) Average normalized fluorescence recovery data of $DNM2^{WT}$-EGFP (black diamonds) and $DNM2^{\Delta DEE}$-EGFP (red dots) of $N = 10$ cells each. (F) Statistical analysis of recovery times obtained by fitting a single exponential association model to each data set. The p value was calculated by the nonparametric Mann−Whitney test. Outliers were excluded according to the Grubbs test. Scale bar, 10 μm.

fragmentation of T-tubules in Drosophila muscle cells.[16] Likewise, expression of the $DNM2^{R465W}$ and $DNM2^{S619L}$ induced the formation of DNM2 aggregates, mislocalization of excitation-contraction (EC) coupling components, destabilization of T-tubules, and impaired muscle function in zebrafish.[36] In contrast, $DNM2^{WT}$ and CMT-associated $DNM2^{G537C}$ did not form large aggregates and did not elicit detectable muscle defects. Interestingly, the S619L mutation, which is found in severe cases of CNM, caused a more profound disruption of normal muscle phenotypes than the more widely expressed but milder R465W mutation. The link between DNM2 hyperactivity and CNM is further highlighted by findings that CNM-like phenotypes are induced upon increased expression of $DNM2^{WT}$ in mice,[37,38] whereas they are reversed upon reduction of DNM2 expression.[39,40] Although the *in vivo* effects of CMT-associated DNM2 mutations have not been as extensively characterized as those of CNM-associated mutations, a key study demonstrated that reduction of DNM2 expression caused impairment of myelination, a characteristic of DNM-dependent CMT.[41] In this context, it is important to note that the gene mutation that generates $DNM2^{\Delta DEE}$ was found to result in dramatic reduction of DNM2 expression.[10]

Our TIRF-FFS experiments revealed that $DNM2^{\Delta DEE}$, like the CNM-associated DNM2 mutants, forms larger peripheral puncta than $DNM2^{WT}$. Using a different approach, live correlative scanning ion conductance microscopy (SICM) coupled with fluorescence confocal microscopy (FCM), Ali et al. addressed similar questions for CNM-associated mutants.[42] They observed that expression of the CNM-associated R465W mutant in Cos-7 cells increases the lifespan of clathrin-coated pits (CCPs) from ∼85 ±25 s in control cells to ∼1932 ±1220 s. Moreover, CCPs formed in the presence of $DNM2^{R465W}$ expanded to a diameter of ∼1 μm diameter. The authors noted that the stability, size, and DNM2 retention of these structures were suggestive of the properties of flat clathrin lattices or "plaques", a possibility that we had also raised in our earlier report.[24] Notably, Ali et al. found that CCPs in fibroblasts from CNM patients heterozygously expressing the R465W mutant at endogenous levels were also larger and more stable than those in control fibroblasts, suggesting that the enlarged PM structures containing mutant DNM2 were not simply the result of overexpression.

The nature of the DNM2-containing cytoplasmic inclusions and their potential contribution to disease remain to be established. We note that aggregate-like DNM2 puncta were previously observed in muscle biopsies from a patient expressing the $DNM2^{D614N}$ CNM mutant[43] and that large intracellular structures containing the CNM-associated $DNM2^{R465W}$ mutant, expressed at approximately endogenous levels, were observed in knock-in mice.[44] For $DNM2^{R369W}$, we also noted the formation of large cytoplasmic inclusions in CV1 cells[24] and, more recently, several other novel CNM-associated DNM2 mutants (G495R, V520G, G624 V, P294L, and R724H) have been linked to the formation of cytoplasmic inclusions in C2C12 cells.[45] The latter study is of particular interest as it demonstrates a strong correlation between the size and stability of aggregates formed by CNM-associated DNM2 variants and their pathogenicity. Likewise, $DNM2^{R465W}$, which causes a mild-to-moderate form of CNM, was shown to form small aggregates along the sarcolemma of transgenic zebrafish, whereas $DNM2^{S619L}$, found in more severe cases of CNM, formed numerous large aggregates located throughout the sarcoplasm.[36] Notably, the CMT-linked mutant $DNM2^{G537C}$ did not form aggregates in the transgenic zebrafish.

It is not clear how deletion of residue $_{555}$DEE$_{557}$ stabilizes DNM2 assemblies. Both the ΔDEE mutation and the well-characterized K562E CMT-linked mutation alter the local electrostatic potential of the PHD, albeit in different directions. By reduction of the net positive charge of loop 3/β-strand 3 of the PHD, the K562E mutation inhibits binding to phosphoinositides and prevents PIP_2-mediated DNM2-self-assembly and GTPase activation. The ΔDEE mutation increases the net positive charge of loop 3 and has no effect on the PIP_2 binding. Increasing the positive charge of the PH

https://doi.org/10.1021/acs.biochem.4c00262
Biochemistry 2024, 63, 2750−2758

domain may account for the reported enhancement of the interaction of DNM2$^{\Delta DEE}$ with microtubules.[31] It has long been accepted that the C-terminal proline/arginine-rich domain (PRD)[46] (specifically residues 746−786 in DNM2[47]) is the major MT binding determinant in dynamins. However, in our early publication highlighting the importance of phosphoinositide interactions with the PH domain for dynamin-dependent endocytosis, we reported that a K535 M mutation in the PH domain of DNM1 also inhibits MT binding.[48] A recent study confirmed the MT-PH domain interaction and demonstrated its disruption by peptides derived from the PH domain.[49] Interestingly, CNM-associated mutations appear to decrease the affinity of DNM2 for MTs.[26]

At present, it is unclear how (or whether) the unique biochemical and biophysical properties of DNM2$^{\Delta DEE}$ cause it to trigger pathogenic mechanisms that differ from those of other CMT-associated mutants, such as DNM2^{K562E}. It would be of interest to determine whether distinct intracellular membrane trafficking pathways are disrupted by DNM2$^{\Delta DEE}$. For example, expression of a CNM-associated DNM2 mutant was found to interfere with autophagy by virtue of its sequestration in high-order complexes with intersectin 1 on the PM.[50] It is possible that expression of DNM2$^{\Delta DEE}$, which, like the CNM-linked mutants, form large, stable puncta on the PM, may have a similar inhibitory effect on autophagy.

■ ASSOCIATED CONTENT

Data Availability Statement

Data will be made available to any interested parties (njames4@hawaii.edu or djameson@hawaii.edu)

Supporting Information

The Supporting Information is available free of charge at https://pubs.acs.org/doi/10.1021/acs.biochem.4c00262.

Supplementary Figure S1: Estimation of the concentration of endogenous DNM2 in HEK293 cells; Supplementary Figure S2: Determination of high and low expression levels for each cell (PDF)

Accession Codes

Accession IDs of proteins used in this study: rat dynamin isoform 1 (also known as isoform "ba" or "IIBA"), UniProtKB identifier P39052−1).

■ AUTHOR INFORMATION

Corresponding Authors

Nicholas G. James − *Department of Cell and Molecular Biology, John A. Burns School of Medicine, University of Hawaii, Honolulu, Hawaii 96813, United States*; Email: njames4@hawaii.edu

David M. Jameson − *Department of Cell and Molecular Biology, John A. Burns School of Medicine, University of Hawaii, Honolulu, Hawaii 96813, United States*; orcid.org/0000-0002-9627-123X; Email: djameson@hawaii.edu

Authors

Per Niklas Hedde − *Beckman Laser Institute and Medical Clinic, Department of Pharmaceutical Sciences, and Department of Biomedical Engineering, University of California, Irvine, California 92697, United States*

Songning Zhu − *Department of Biomedical Engineering, University of California, Irvine, California 92697, United States*

Barbara Barylko − *Department of Pharmacology, University of Texas Southwestern Medical Center, Dallas, Texas 75390-9041, United States*

Chi-Li Chiu − *Department of Biomedical Engineering, University of California, Irvine, California 92697, United States*

Luke T. Nelson − *Department of Cell and Molecular Biology, John A. Burns School of Medicine, University of Hawaii, Honolulu, Hawaii 96813, United States*

Michelle A. Digman − *Department of Biomedical Engineering, University of California, Irvine, California 92697, United States*; orcid.org/0000-0003-4611-7100

Joseph P. Albanesi − *Department of Pharmacology, University of Texas Southwestern Medical Center, Dallas, Texas 75390-9041, United States*; orcid.org/0000-0002-6864-8140

Complete contact information is available at: https://pubs.acs.org/10.1021/acs.biochem.4c00262

Author Contributions

All authors have contributed to writing the manuscript. N.G.J., M.D., D.M.J., and J.P.A. were responsible for the experimental design. P.N.H. performed imaging and photobleaching experiments. C-L.C. performed 3D orbital tracking experiments. B.B. created fusion constructs, and S.Z. performed imaging and spot size analyses.

Funding

This research was funded by NIH grants GM123048−02 (N.G.J.), MH119516 (D.M.J. and J.P.A.), and NSF-1847005 (M.A.D.).

Notes

The authors declare no competing financial interest.

■ ACKNOWLEDGMENTS

Imaging and particle tracking were performed at the Laboratory for Fluorescence Dynamics (LFD) at the University of California, Irvine (UCI). The LFD was supported jointly by the National Institute of General Medical Sciences of the National Institutes of Health (P41GM103540), and UCI.

■ REFERENCES

(1) Chappie, J. S.; Dyda, F. Building a fission machine − structural insights into dynamin assembly and activation. *J. Cell Sci.* **2013**, *126*, 2773−2784.

(2) Morlot, S.; Roux, A. Mechanics of dynamin-mediated membrane fission. *Annu. Rev. Biophys.* **2013**, *42*, 629−49.

(3) Menon, M.; Schafer, D. A. Dynamin: expanding its scope to the cytoskeleton. *Int. Rev. Cell Mol. Biol.* **2013**, *302*, 187−219.

(4) Sever, S.; Chang, J.; Gu, C. Dynamin rings: not just for fission. *Traffic* **2013**, *14*, 1194−1199.

(5) Cao, H.; Garcia, F.; McNiven, M. A. Differential distribution of dynamin isoforms in mammalian cells. *Mol. Biol. Cell* **1998**, *9*, 2595−2609.

(6) Ferguson, S. M.; De Camilli, P. Dynamin, a membrane-remodelling GTPase. *Nat. Rev. Mol. Cell Biol.* **2012**, *13*, 75−88.

(7) Faelber, K.; Posor, Y.; Gao, S.; Held, M.; Roske, Y.; Schulze, D.; Haucke, V.; Noe, F.; Daumke, O. Crystal structure of nucleotide-free dynamin. *Nature* **2011**, *477*, 556−560.

(8) Ford, M. G.; Jenni, S.; Nunnari, J. The crystal structure of dynamin. *Nature* **2011**, *477*, 561−566.

(9) Srinivasan, S.; Dharmarajan, V.; Reed, D. K.; Griffin, P. R.; Schmid, S. L. Identification and function of conformational dynamics in the multidomain GTPase dynamin. *EMBO J.* **2016**, *35*, 443−457.

(10) Züchner, S.; Noureddine, M.; Kennerson, M.; Verhoeven, K.; Claeys, K.; Jonghe, P. D.; Merory, J.; Oliveira, S. A.; Speer, M. C.; Stenger, J. E.; Walizada, G.; Zhu, D.; Pericak-Vance, M. A.; Nicholson, G.; Timmerman, V.; Vance, J. M. Mutations in the pleckstrin homology domain of dynamin 2 cause dominant intermediate Charcot-Marie-Tooth disease. *Nat. Genet.* **2005**, *37*, 289−294.
(11) González-Jamett, A. M.; Haro-Acuña, V.; Momboisse, F.; Caviedes, P.; Bevilacqua, J. A.; Cárdenas, A. M. Dynamin-2 in nervous system disorders. *J. Neurochem.* **2014**, *128*, 210−223.
(12) Bitoun, M.; Maugenre, S.; Jeannet, P. Y.; Lacene, E.; Ferrer, X.; Laforet, P.; Martin, J. J.; Laporte, J.; Lochmuller, H.; Beggs, A. H.; Fardeau, M.; Eymard, B.; Romero, N. B.; Guicheney, P. Mutations in dynamin 2 cause dominant centronuclear myopathy. *Nat. Genet.* **2005**, *37*, 1207−1209.
(13) Zhao, M.; Maani, N.; Dowling, J. J. Dynamin 2 (DNM2) as cause of, and modifier for, human neuromuscular disease. *Neurotherapeutics* **2018**, *15*, 966−975.
(14) Wang, L.; Barylko, B.; Byers, C.; Ross, J. A.; Jameson, D. M.; Albanesi, J. P. Dynamin 2 mutants linked to centronuclear myopathies form abnormally stable polymers. *J. Biol. Chem.* **2010**, *285*, 22753−22757.
(15) Kenniston, J. A.; Lemmon, M. A. Dynamin GTPase regulation is altered by PH domain mutations found in centronuclear myopathy patients. *EMBO J.* **2010**, *29*, 3054−3067.
(16) Chin, Y. H.; Lee, A.; Kan, H. W.; Laiman, J.; Chuang, M. C.; Hsieh, S. T.; Liu, Y. W. Dynamin-2 mutations associated with centronuclear myopathy are hypermorphic and lead to T-tubule fragmentation. *Hum. Mol. Genet.* **2015**, *24*, 5542−5554.
(17) Muñoz, X. M.; Buono, S.; Koebel, P.; Laporte, J.; Cowling, B. S. Different in vivo impacts of dynamin 2 mutations implicated in Charcot-Marie-Tooth neuropathy or centronuclear myopathy. *Hum. Mol. Genet.* **2019**, *28*, 4067−4077.
(18) Gomez-Oca, R.; Cowling, B. S.; Laporte, J. Common pathogenic mechanisms in centronuclear and myotubular myopathies and latest treatment advances. *Int. J. Mol. Sci.* **2021**, *22*, 11377.
(19) Bitoun, M.; Bevilacqua, J. A.; Prudhon, B.; Maugenre, S.; Taratuto, A. L.; Monges, S.; Lubieniecki, F.; Cances, C.; Uro-Coste, E.; Mayer, M.; Fardeau, M.; Romero, N. B.; Guicheney, P. Dynamin 2 mutations cause sporadic centronuclear myopathy with neonatal onset. *Ann. Neurol.* **2007**, *62*, 666−670.
(20) Laiman, J.; Lin, S. S.; Liu, Y. W. Dynamins in human diseases: differential requirement of dynamin activity in distinct tissues. *Curr. Opin. Cell Biol.* **2023**, *81*, No. 102174.
(21) Tassin, T. C.; Barylko, B.; Hedde, P. N.; Chen, Y.; Binns, D. D.; James, N. G.; Mueller, J. D.; Jameson, D. M.; Taussig, R.; Albanesi, J. P. Gain-of-function properties of a dynamin 2 mutant implicated in Charcot-Marie-Tooth Disease. *Front. Cell. Neurosci.* **2021**, *15*, No. 745940.
(22) Chiu, C. L.; Digman, M. A.; Gratton, E. Measuring actin flow in 3D cell protrusions. *Biophys. J.* **2013**, *105*, 1746−1755.
(23) Lanzanò, L.; Gratton, E. Orbital Single Particle Tracking on a commercial confocal microscope using piezoelectric stage feedback. *Methods Appl. Fluoresc.* **2014**, *2* (2), No. 024010.
(24) James, N. G.; Digman, M. A.; Ross, J. A.; Barylko, B.; Wang, L.; Li, J.; Chen, Y.; Mueller, J. D.; Gratton, E.; Albanesi, J. P.; Jameson, D. M. A mutation associated with centronuclear myopathy enhances the size and stability of dynamin 2 complexes in cells. *Biochim. Biophys. Acta* **2014**, *1840*, 315−321.
(25) Bayonés, L.; Guerra-Fernández, M. J.; Hinostroza, F.; Báez-Matus, X.; Vásquez-Navarrete, J.; Gallo, L. I.; Parra, S.; Martínez, A. D.; González-Jamett, A.; Marengo, F. D.; Cárdenas, A. M. Gain-of-function dynamin-2 mutations linked to centronuclear myopathy impair Ca2+-induced exocytosis in human myoblasts. *Int. J. Mol. Sci.* **2022**, *23*, 10363.
(26) Koutsopoulos, O. S.; Koch, C.; Tosch, V.; Böhm, J.; North, K. N.; Laporte, J. Mild functional differences of dynamin 2 mutations associated to centronuclear myopathy and Charcot-Marie-Tooth peripheral neuropathy. *PLoS One* **2011**, *6* (11), No. e27498.
(27) Sambuughin, N.; Goldfarb, L. G.; Sivtseva, T. M.; Davydova, T. K.; Vladimirtsev, V. A.; Osakovskiy, V. L.; Danilova, A. P.; Nikitina, R. S.; Ylakhova, A. N.; Diachkovskaya, M. P.; Sundborger, A. C.; Renwick, N. M.; Platonov, F. A.; Hinshaw, J. E.; Toro, C. Adult-onset autosomal dominant spastic paraplegia linked to a GTPase-effector domain mutation of dynamin 2. *BMC Neurol.* **2015**, *15*, 223.
(28) Itzhak, D. N.; Tyanova, S.; Cox, J.; Borner, G. H. Global, quantitative and dynamic mapping of protein subcellular localization. *Elife* **2016**, *5*, No. e16950.
(29) Ross, J. A.; Digman, M. A.; Wang, L.; Gratton, E.; Albanesi, J. P.; Jameson, D. M. Oligomerization state of dynamin 2 in cell membranes using TIRF and number and brightness analysis. *Biophys. J.* **2011**, *100*, L15−L17.
(30) Sidiropoulos, P. N.; Miehe, M.; Bock, T.; Tinelli, E.; Oertli, C. I.; Kuner, R.; Meijer, D.; Wollscheid, B.; Niemann, A.; Suter, U. Dynamin 2 mutations in Charcot-Marie-Tooth neuropathy highlight the importance of clathrin-mediated endocytosis in myelination. *Brain.* **2012**, *135*, 1395−1411.
(31) Tanabe, K.; Takei, K. Dynamic instability of microtubules requires dynamin 2 and is impaired in a Charcot-Marie-Tooth mutant. *J. Cell Biol.* **2009**, *185*, 939−948.
(32) Bitoun, M.; Durieux, A. C.; Prudhon, B.; Bevilacqua, J. A.; Herledan, A.; Sakanyan, V.; Urtizberea, A.; Cartier, L.; Romero, N. B.; Guicheney, P. Dynamin 2 mutations associated with human diseases impair clathrin-mediated receptor endocytosis. *Hum. Mutat.* **2009**, *30*, 1419−1427.
(33) Liu, Y. W.; Lukiyanchuk, V.; Schmid, S. L. Common membrane trafficking defects of disease-associated dynamin 2 mutations. *Traffic* **2011**, *12*, 1620−1633.
(34) Yamada, H.; Kobayashi, K.; Zhang, Y.; Takeda, T.; Takei, K. Expression of a dynamin 2 mutant associated with Charcot-Marie-Tooth disease leads to aberrant actin dynamics and lamellipodia formation. *Neurosci. Lett.* **2016**, *628*, 179−85.
(35) Hamasaki, E.; Wakita, N.; Yasuoka, H.; Nagaoka, H.; Morita, M.; Takashima, E.; Uchihashi, T.; Takeda, T.; Abe, T.; Lee, J. W.; Iimura, T.; Saleem, M. A.; Ogo, N.; Asai, A.; Narita, A.; Takei, K.; Yamada, H. The lipid-binding defective dynamin 2 mutant in Charcot-Marie-Tooth disease impairs proper actin bundling and actin organization in glomerular podocytes. *Front. Cell Dev. Biol.* **2022**, *10*, No. 884509.
(36) Zhao, M.; Smith, L.; Volpatti, J.; Fabian, L.; Dowling, J. J. Insights into wild-type dynamin 2 and the consequences of DNM2 mutations from transgenic zebrafish. *Hum. Mol. Genet.* **2019**, *28*, 4186−4196.
(37) Cowling, B. S.; Toussaint, A.; Amoasii, L.; Koebel, P.; Ferry, A.; Davignon, L.; Nishino, I.; Mandel, J. L.; Laporte, J. Increased expression of wild-type or a centronuclear myopathy mutant of dynamin 2 in skeletal muscle of adult mice leads to structural defects and muscle weakness. *Am. J. Pathol.* **2011**, *178*, 2224−2235.
(38) Liu, N.; Bezprozvannaya, S.; Shelton, J. M.; Frisard, M. I.; Hulver, M. W.; McMillan, R. P.; Wu, Y.; Voelker, K. A.; Grange, R. W.; Richardson, J. A.; Bassel-Duby, R.; Olson, E. N. Mice lacking microRNA 133a develop dynamin 2-dependent centronuclear myopathy. *J. Clin. Invest.* **2011**, *121*, 3258−3268.
(39) Cowling, B. S.; Chevremont, T.; Prokic, I.; Kretz, C.; Ferry, A.; Coirault, C.; Koutsopoulos, O.; Laugel, V.; Romero, N. B.; Laporte, J. Reducing dynamin 2 expression rescues X-linked centronuclear myopathy. *J. Clin. Invest.* **2014**, *124*, 1350−1363.
(40) Buono, S.; Ross, J. A.; Tasfaout, H.; Levy, Y.; Kretz, C.; Tayefeh, L.; Matson, J.; Guo, S.; Kessler, P.; Monia, B. P.; Bitoun, M.; Ochala, J.; Laporte, J.; Cowling, B. S. Reducing dynamin 2 (DNM2) rescues DNM2-related dominant centronuclear myopathy. *Proc. Natl. Acad. Sci. U.S.A.* **2018**, *115*, 11066−11071.
(41) Gerber, D.; Ghidinelli, M.; Tinelli, E.; Somandin, C.; Gerber, J.; Pereira, J. A.; Ommer, A.; Figlia, G.; Miehe, M.; Nageli, L. G.; Suter, V.; Tadini, V.; Sidiropoulos, P. N.; Wessig, C.; Toyka, K. V.; Suter, U. Schwann cells, but not Oligodendrocytes, Depend Strictly on Dynamin 2 Function. *Elife* **2019**, *8*, No. e42404.

https://doi.org/10.1021/acs.biochem.4c00262
Biochemistry 2024, 63, 2750−2758

(42) Ali, T.; Bednarska, J.; Vassilopoulos, S.; Tran, M.; Diakonov, I. A.; Ziyadeh-Isleem, A.; Guicheney, P.; Gorelik, J.; Korchev, Y. E.; Reilly, M. M.; Bitoun, M.; Shevchuk, A. Correlative SICM-FCM reveals changes in morphology and kinetics of endocytic pits induced by disease-associated mutations in dynamin. *FASEB J.* **2019**, *33*, 8504−8518.
(43) Kierdaszuk, B.; Berdynski, M.; Karolczak, J.; Redowicz, M. J.; Zekanowski, C.; Kaminska, A. M. A novel mutation in the DNM2 gene impairs dynamin 2 localization in skeletal muscle of a patient with late onset centronuclear myopathy. *Neuromuscul. Disord.* **2013**, *23*, 219−228.
(44) Durieux, A. C.; Vignaud, A.; Prudhon, B.; Viou, M. T.; Beuvin, M.; Vassilopoulos, S.; Fraysse, B.; Ferry, A.; Laine, J.; Romero, N. B.; Guicheney, P.; Bitoun, M. A centronuclear myopathy-dynamin 2 mutation impairs skeletal muscle structure and function in mice. *Hum. Mol. Genet.* **2010**, *19*, 4820−4836.
(45) Fujise, K.; Okubo, M.; Abe, T.; Yamada, H.; Takei, K.; Nishino, I.; Takeda, T.; Noguchi, S. Imaging-based evaluation of pathogenicity by novel DNM2 variants associated with centronuclear myopathy. *Hum. Mutat.* **2022**, *43*, 169−179.
(46) Tuma, P. L.; Stachniak, M. C.; Collins, C. A. Activation of dynamin GTPase by acidic phospholipids and endogenous rat brain vesicles. *J. Biol. Chem.* **1993**, *268*, 17240−17246.
(47) Hamao, K.; Morita, M.; Hosoya, H. New function of the proline rich domain in dynamin-2 to negatively regulate its interaction with microtubules in mammalian cells. *Exp. Cell Res.* **2009**, *315*, 1336−1345.
(48) Achiriloaie, M.; Barylko, B.; Albanesi, J. P. Essential role of the dynamin pleckstrin homology domain in receptor-mediated endocytosis. *Mol. Cell. Biol.* **1999**, *19*, 1410−145.
(49) Hori, T.; Eguchi, K.; Wang, H. Y.; Miyasaka, T.; Guillaud, L.; Taoufiq, Z.; Mahapatra, S.; Yamada, H.; Takei, K.; Takahashi, T. Microtubule assembly by tau impairs endocytosis and neurotransmission via dynamin sequestration in Alzheimer's disease synapse model. *Elife* **2022**, *11*, No. e73542.
(50) Puri, C.; Manni, M. M.; Vicinanza, M.; Hilcenko, C.; Zhu, Y.; Runwal, G.; Stamatakou, E.; Menzies, F. M.; Mamchaoui, K.; Bitoun, M.; Rubinsztein, D. C. A DNM2 centronuclear myopathy mutation reveals a link between recycling endosome scission and autophagy. *Dev. Cell.* **2020**, *53*, 154−168.e6.

https://doi.org/10.1021/acs.biochem.4c00262
Biochemistry 2024, 63, 2750−2758